Design of Industrial Axial Compressor Blade Sections for Optimal Range and Performance

Frank Sieverding
Sulzer Innotec,
Sulzer Markets and Technology,
CH-8401 Winterthur, Switzerland

Beat Ribi
MAN Turbomaschinen AG Schweiz,
Hardstrasse 319,
CH-8005 Zurich, Switzerland

Michael Casey
Institut für Thermische
Strömungsmaschinen (ITSM),
Universität Stuttgart,
D-70569 Stuttgart, Germany

Michael Meyer
MAN Turbomaschinen AG Schweiz,
Hardstrasse 319,
CH-8005 Zurich, Switzerland

Background: The blade sections of industrial axial flow compressors require a wider range from surge to choke than typical gas turbine compressors in order to meet the high volume flow range requirements of the plant in which they operate. While in the past conventional blade profiles (NACA65 or C4 profiles) at moderate Mach number have mostly been used, recent well-documented experience in axial compressor design for gas turbines suggests that peak efficiency improvements and considerable enlargement of volume flow range can be achieved by the use of so-called prescribed velocity distribution (PVD) or controlled diffusion (CD) airfoils. Method of approach: The method combines a parametric geometry definition method, a powerful blade-to-blade flow solver and an optimization technique (breeder genetic algorithm) with an appropriate fitness function. Particular effort has been devoted to the design of the fitness function for this application which includes non-dimensional terms related to the required performance at design and off-design operating points. It has been found that essential aspects of the design (such as the required flow turning, or mechanical constraints) should not be part of the fitness function, but need to be treated as so-called "killer" criteria in the genetic algorithm. Finally, it has been found worthwhile to examine the effect of the weighting factors of the fitness function to identify how these affect the performance of the sections. Results: The system has been tested on the design of a repeating stage for the middle stages of an industrial axial compressor. The resulting profiles show an increased operating range compared to an earlier design using NACA65 profiles. Conclusions: A design system for the blade sections of industrial axial compressors has been developed. Three-dimensional CFD simulations and experimental measurements demonstrate the effectiveness of the new profiles with respect to the operating range. [DOI: 10.1115/1.1737782]

Introduction

The blade sections of industrial axial flow compressors require a wider range from surge to choke than typical gas turbine compressors in order to meet the high-volume flow-range requirements of the plant in which they operate. For motor-driven units it is often necessary to have a large number of variable stators to meet these requirements. In addition, the compressors are usually assembled from a limited set of standardized stages and casings to meet the particular customer specifications. These can vary substantially from machine to machine to cope with completely different requirements in terms of mass flow, pressure ratio and gas properties—and therefore of rotor size, number of stages, Mach numbers, and Reynolds numbers.

It is normal practice in such compressors to use so-called repeating stages, whereby several successive stages have the same blades for the rotors and stators but the span of the blade rows are shortened by cropping the tips. The requirements of axial matching determines the local meridional flow channel and defines the height of the blades, see Goede and Casey [1]. Normally there are different styles of repeating stage design for the front, middle, and end stages, whereby the following design criteria are used for these:

Front stages

- insensitive to high Mach number
- sensitive to variable IGV setting angles
- low hub/tip ratio

Middle stages

- high efficiency
- high work input per stage
- wide range without variables

End stages

- low flow coefficient giving high span
- low exit swirl

In general these requirements lead to designs of 50 to 60% reaction stages at the front, 70 to 80% in the middle and zero swirl (90% reaction) at the end. The stage in consideration in this paper is in the middle section of the compressor, where more or less sound repeating conditions are given.

This type of standardization of the design forbids several design features that are often encountered in axial compressors for gas turbines. Transonic blades are excluded, as the operating range would be too small and the axial matching of the sections would be too sensitive to cropping. The variation of blade height through cropping also impedes a refinement of the aerodynamics in the endwall region, although a treatment of the blade roots alone could be considered. The shift of the rotor and stator blade sections relative to each other through cropping (the rotor is shortened from the casing section and the stator from the hub section) also precludes any fine optimization of the design through the axial matching of the blade sections. To alleviate this problem, the middle stage considered here is designed with a constant exit flow angle from the stator across the span. Any improvement in performance is therefore primarily focused on the reduction of profile losses and improvement of the operating range of the section to allow it to cope with the severe aerodynamic maltreatment through cropping.

For this type of axial compressor, conventional blade profiles (NACA65 or C4 profiles) at moderate Mach number have mostly

Contributed by the International Gas Turbine Institute and presented at the International Gas Turbine and Aeroengine Congress and Exhibition, Atlanta, GA, June 16–19, 2003. Manuscript received by the IGTI December 2002; final revision March 2003. Paper No. 2003-GT-38036. Review Chair: H. R. Simmons.

been used as the availability of well-documented correlations allow the influence of changes in design parameters to be assessed with ease (Casey [2] and Casey and Hugentobler [3]). However, recent well-documented experience in axial compressor design for gas turbines suggests that peak efficiency improvements and considerable enlargement of volume flow range can be achieved by the use of so-called prescribed velocity distribution (PVD) or controlled diffusion (CD) airfoils. These types of bade sections are already widely used in compressors in jet engines and in stationary gas turbines and have also been applied in industrial compressors (Eisenberg [4]). Hobbs and Weingold [5] describe several features of the profiles whose advantages over conventional profiles have been proven. These features can be summarized as follows (see also Cumpsty [6]):

- a very rapid acceleration near the leading edge to avoid premature laminar boundary layer separation or transition,
- a deceleration region, beginning very steep, but relaxing so as to keep the boundary layer form parameter H_k approximately constant, and
- for the pressure side a nearly constant subsonic Mach number distribution.

The most promising approach for the design of controlled diffusion style of airfoils has been documented in two recent ASME papers by DLR and Siemens (Köller et al. [7] and Küsters et al. [8]) and this paper documents the transfer and adaptation of this technology to industrial compressors.

Description of Design System

The blade shapes of PVD or CD profiles are almost arbitrary and the number of degrees-of-freedom is high so an efficient design system without correlations is called for. A design system consisting of a parameterized geometry description, a fast two-dimensional flow solver and an optimization tool has proved to be an efficient way to evaluate the optimal set of parameters for given boundary conditions. Due to the two-dimensional optimization, three-dimensional effects such as secondary flow and tip leakage flow are neglected. This concession has to be made as the available three-dimensional Navier-Stokes codes are still too time-consuming to be coupled with optimization algorithms, although three-dimensional Euler codes which are adequate for water turbine designs can be incorporated, see Sallaberger et al. [9]. Instead, the three-dimensional geometry of the blade is defined by the radial stacking of three planar sections (hub, root-mean-square (rms), and casing), each of which is optimized separately using the procedure shown in **Fig. 1**.

The geometry of one section is defined by a set of parameters given by the genetic algorithm (i.e., breeder genetic algorithm (BGA)). Once the geometry has been generated by the geometry program (GEOM), preliminary checks are performed to ensure that vital mechanical aspects such as cross section area, moment of inertia or limitations concerning the curvature of the blade shape are not violated. If any of these checks is not passed successfully, the individual is marked as a ''bad'' individual and no further evaluation is done—it is effectively killed off without further consideration. Similarly, designs which do not achieve the required outlet flow angle—and therefore violate the specific work and flow turning required for the axial matching of the sections—are also eliminated by this ''killer'' criteria.

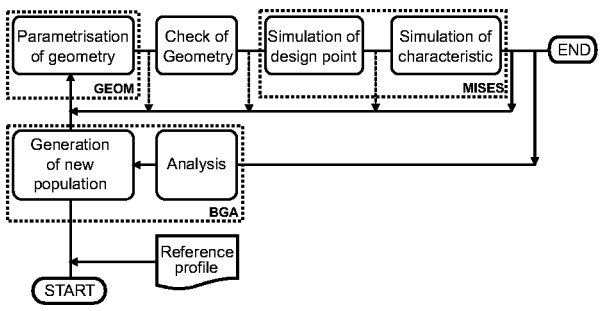

Fig. 1 Design system

Optimizing with respect to the whole characteristic (at design and off-design operating points) strongly increases the turnaround time for one optimization. The calculations of the characteristic are conducted up to an operating point that shows a doubled profile loss compared to the design point. To reduce the effort, the flow simulation is split into two steps, the simulation of the design point (i.e., evaluating of the exit flow angle at the design point) and—only if the exit flow angle is within the given limits—the simulation of the characteristic. Nevertheless, the elapsed time for a complete section is, in the worst case, about 14 days.

In this case, the development of a new blade sections is based on an already existing design (NACA65) which is to be improved. A reference profile, which closely represents the current design, is included in the optimization process in the start population to ensure that current knowhow and experience are taken into account. Although this might accelerate the process of optimization, it is important to note that it does not affect the result of the optimization itself. Test runs have led to the same result with and without including the reference profile.

Parameterization of Blade Section Geometry

The challenge for the geometry program is to provide an accurate and flexible parameterization by using a low number of parameters so as the effort of optimizing is reduced. The implemented solution uses the concept of superposition of a camber line and a thickness distribution. This was necessary so that the new sections could be incorporated into the available design system which uses this technique, following Casey [10]. Both distributions are described by four patches, two central Bezier patches of order 4 and two linear patches for the leading and the trailing edge (see **Fig. 2**). In case of the thickness distribution the leading edge patch is replaced by an ellipse.

Altogether, the geometry model ends up with 20 parameters, 10 for the camber line and 10 for the thickness distribution for each blade section. Each parameter is directly or indirectly related to the chord length. By scaling with the chord length, the final design can therefore easily be obtained.

Some of the parameters are not object of the optimization, such as the chord length and the trailing edge radius (actually rTE/c), others are restricted or used as an initial value, such as the parameters p7 to p10, because they are not independent of each other. With the parameters p3 and p5 position and slope of the first point of patch 2 are defined. The position of the last point of patch 2 is

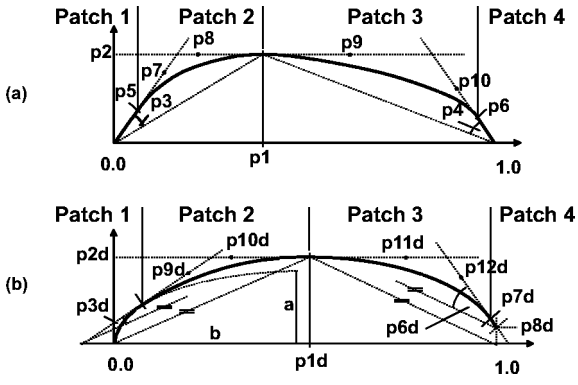

Fig. 2 Parameterization of (*a*) camber line and (*b*) thickness distribution

given by p1 and p2 and, as this is the point of maximal camber, the slope is also known. Parameters p7 and p8 finally specify the inner polygon points. In the same manner, the second Bezier patch (i.e., patch 3) is described. Arbitrary combinations of the parameters p1 to p10 will result in a discontinuity of the curvature at the transition of patch 2 to 3. Therefore p7 to p10 are varied in an internal loop until continuity of the curvature is achieved.

What has so far been described for the camber line, is also true for the thickness distribution, save that the first polygon point of patch 2 is defined as the location at which the ellipse with a minor to major axis ratio of 0.3 shows the same slope as p3d.

Two-Dimensional Flow Solver

The quasi-three-dimensional blade-to-blade solver MISES V2.4.1 (Youngren and Drela [11]) has been chosen as the flow code for the optimization. This fast code describes the inviscid flow using the steady Euler equations, while the viscous effects are modeled by the integral boundary layer equations. The coupled system of nonlinear equations is solved by a Newton-Raphson technique.

The boundary conditions are defined by those of the existing NACA stage. Beginning at the design point the inlet angle is varied while keeping the inlet Mach number constant. For the stages in consideration the turbulence level is typically 5% and higher. According to Abu-Ghannam and Shaw [12], there is no further influence of turbulence on bypass transition for levels above 3%, so that the turbulence level is set to 5%.

For all calculations the radius of the section is taken as constant and the AVDR is set to unity, which means that both, stator and rotor sections, can be optimized with no rotation. Adjustments for noncylindrical flow channel and therefore nonconstant radius and AVDR$>$1 are made by modification of the desired exit flow angle.

Breeder Genetic Algorithm

The breeder genetic algorithm (BGA), developed by Mühlenbein and Schlierkamp-Voosen [13,14], is based on the evolution theories of Darwin and the genetics of Mendel. A population of individuals changes over a number of generations using the mechanisms of selection, recombination and mutation, whereby the best individual is always transferred unchanged to the next generation (elitism).

According to the findings of former projects using this optimization tool (see Sallaberger [9] for details) the parameters for the optimization process were chosen to be 0.20 for the selection threshold, $[-0.20,1.20]$ for the recombination interval and $[-0.25,0.25]$ for the mutation interval. Starting with a population size of 500 individuals, each following generation consists of 50 individuals, which compromises the calculation time for one generation and the number of generations needed until the optimum is found.

It is worth noting here that the stringent convergence criteria applied in the optimization process (see below) indicate that a true optimum is found, and in this sense the results are independent of the actual optimization algorithm that is used. Other systems of optimization have been examined (including gradient methods and neural networks) but none were found to be consistently better than the breeder genetic algorithm.

Fitness Function

Experience obtained from former projects has led to the following conclusions:

- Every term of the fitness function has to be associated to suitable reference values so that the contributions to the fitness value are all of the same order of magnitude.
- The distinction has to be made between goals which are essential and goals which are desirable. Only the latter should be included in the fitness function.

Fig. 3 Influence of moment of inertia on resulting profiles (dashed line: original; solid line: cross section area and moment of inertial taken into account)

Typically, the terms of the fitness function are of different types, like loss coefficients or angles. Without relating them to reference values, the numerical values of flow angles (in units of degrees) would outweigh any improvement in the loss coefficient (typically 0.03), as long as it is not compensated by a well-chosen weighting factor. With reference values each component in the fitness function has the same order of magnitude and the choice of appropriate weighting factors is much simplified. Suitable reference values can be obtained from experience or from existing profiles.

By definition, essential criteria have to be fulfilled without exception. If they were included in the fitness function, their corresponding weighting factors would have to be set at very high levels, and—as explained above—the criteria would become so dominant that required criteria would no longer be relevant. This type of criteria is called ''killer criteria'' and checked beforehand.

In the present case of an industrial axial compressor four killer criteria have been identified:

- the exit flow angle,
- the moment of inertia,
- the cross-section area, and
- the number of turning points on suction and pressure side.

The first of these is related to the achievement of the required specific work and appropriate axial matching of the sections, and, the second and third take into account the bending and centrifugal stresses, and the fourth is related to manufacturing requirements.

Strictly speaking, the cross-section area concerns only the rotor, but in order to develop a standardized method for rotor and stator it is checked for the stator as well. The effect of taking into account the cross section area and the moment of inertia is demonstrated in **Fig. 3**. Optimizing without these criteria leads to a profile with little camber, with the maximum thickness close to the leading edge and a very thin trailing edge. On the other hand, the resulting profile with respect to the stress criteria shows increased camber and a more regular thickness distribution. The previous shape might be superior in terms of loss coefficient and operating range, but is of no technical interest.

So far the exit flow angle has been described and classified as a killer criteria. This classification will now be examined in more detail. A design which meets the exact exit flow angle is only an

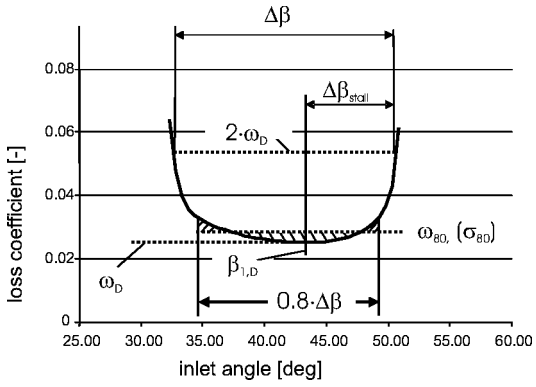

Fig. 4 Parameter of the characteristic for the evaluation by the fitness function

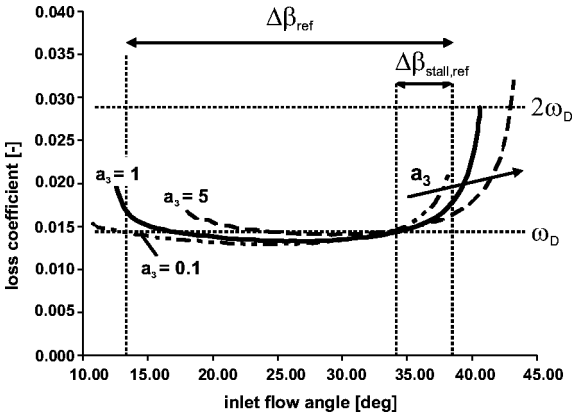

Fig. 5 Influence of weighting factor a_3 on $\Delta\beta_{stall}$

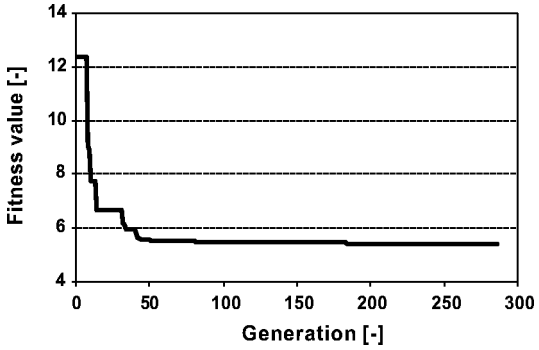

Fig. 6 "Convergence" behavior of the optimization process of the stator casing section

academic task, the designer will rather allow a defined tolerance, especially as the methods for prediction of exit angle are not perfect. Thus, we have to distinguish between two cases. If the exit flow angle is outside of the specified tolerance, it is interpreted as a killer criteria and therefore the affected individuals excluded. But, if the exit flow angle is within the tolerance, it is no longer a killer criteria. On the contrary, the exit flow angle is now an object of the optimization to meet the requirements as accurate as possible. For this reason, it is part of the fitness function, but the fitness value is only analyzed for those individuals whose exit flow angle is within the tolerance.

The components of the fitness function to describe position and shape of the characteristic have been chosen according to the proposal of Köller et al. [7] and are sketched in **Fig. 4**. For the design point $\beta_{1,D}$ the profile shows a design loss coefficient of ω_D. When decreasing or increasing the inlet flow angle, the losses will eventually start to rise until a loss coefficient double that of the design point is reached. This range is defined as the operating range and the difference between the stall point and the design point is known as the safety against stall. For the inner 80% of the operating range the average value ω_{80} and the standard deviation σ_{80} are used to assess the flatness and the homogenity of the loss characteristic.

Altogether, the fitness function consists of 6 components

$$F = a_1\left(\frac{\omega_D}{\omega_{D,\mathrm{ref}}}\right)^{e_1} + a_2\left(\frac{\Delta\beta_{\mathrm{ref}}}{\Delta\beta}\right)^{e_2} + a_3\left(\frac{\Delta\beta_{\mathrm{stall,ref}}}{\Delta\beta_{\mathrm{stall}}}\right)^{e_3} + a_4\left(\frac{\omega_{80}}{\omega_{80,\mathrm{ref}}}\right)^{e_4} + a_5\left(\frac{\sigma_{80}}{\sigma_{80,\mathrm{ref}}}\right)^{e_5} + a_6\left(1+\left|\frac{\beta_2-\beta_{2,\mathrm{ref}}}{\beta_{2,\mathrm{ref}}}\right|\right)^{e_6} \quad (1)$$

whereby ref refers to values of the reference profile used to make each term nondimensional. It is interesting to note that because the blade-to-blade code of MISES is able to predict the operating range and the loss coefficients, there are no elements of the fitness function which are related to the specification of optimum velocity distributions or boundary layer distributions.

Each component is associated with a weighting factor a_i and an exponent e_i. The exponent factors e_i have not been used and are all set to unity. It has been found expedient to examine the influence of each of the weighting factors a_i separately. As an example, the influence of a_3 (responsible for the safety against stall) is shown in **Fig. 5**.

Increasing the weighting factor a_3 gives a higher margin against stall through an increased stagger angle and leads to less incidence for high inlet flow angles. Furthermore, the leading edge is thickened, so that the profile is less sensitive to incidence. Both measures improve the safety against stall. On the other side, due to the higher incidence for small inlet flow angles, the losses are increased and the operating range towards choke is substantially reduced.

It is interesting to note here that studies of the effect of the weighting factors a_4 and a_5 did not substantially affect the design of the sections, indicating that the fullness and the width of the characteristic close to low loss is probably similar for all axial compressor sections and is related to the global features of the flow rather than detail of the profile shape.

Time Frame of Optimization Process

The optimization process is regarded as "converged," if the best individual has not changed for more than 70 generations or the 400th generation is reached (see **Fig. 6**). There can, of course, be no proof that with more generations a better individual would not be found. To test the risk of this, several sections have been optimized starting from different reference profiles and, with the convergence criteria given above, no differences in the optimized profile could be identified even when starting from quite different starting profiles.

This optimization process for one section typically requires about two weeks on a single DEC ALPHA ES40 processor, whereby the characteristic is only calculated if all geometrical requirements are fulfilled and the exit flow angle is within the given limits for the design point.

The time frame strongly depends on the section that is to be optimized. Rotor sections generally take longer than stator sections. This is due to the boundary conditions (higher Mach numbers) which require longer convergence times in MISES (especially if shocks occur). The system has not been made parallel to improve its speed, but on a multiprocessor machine different blade sections can be optimized in different processors at the same time.

Results of Optimization of Sections

The features of the optimized sections are in good agreement with the expected velocity profiles and boundary layer development expected for PVD and CD profiles (see introduction), even though no specific aspect of the fitness function is related to velocity distributions or boundary layer parameters. Clearly, the physics of the flow included in MISES is able to identify that the typical velocity boundary layer distributions automatically minimize the fitness function chosen, which examines only losses and operating range.

One example of the results for the casing section of the stator is given in **Figs. 7–11**. In these comparisons the reference data are the MISES calculation for the original NACA profile. In many cases the MISES simulation identifies problems that occur in this reference section that could probably have been avoided by using a different NACA65 profile with different camber and stagger. The original design was carried out without the MISES results using the procedure outlined by Casey and Hugentobler [3] so that the improvements given by the optimization process include some effects due to the poor selection of the original reference profile.

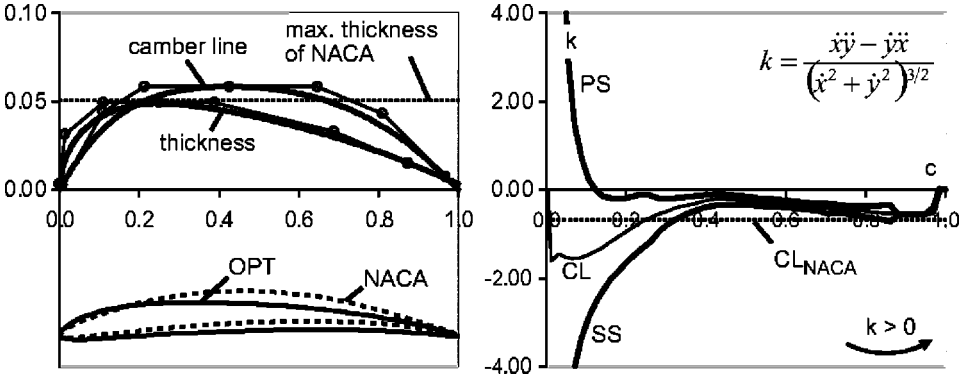

Fig. 7 Stator casing section. Camber and thickness distribution showing polygon points (upper left), geometry without stagger (lower left), and curvature (right).

Geometric Features. On the right side of **Fig. 7** the curvature of the optimized camber line (CL) is compared with that of the NACA profile whose camber is approximately a circular arc. The curvature in the front part of the optimized profile is increased, while it is less over the rear 75% of the section, leading to the typical shape of CD profiles with a relatively low curvature towards the rear of the blade. Additionally, the location of the maximum thickness, which is at 40% of the chord length for the NACA profile, has been moved forwards (**Fig. 7** upper left) and is now very close to its lower limit of 25% chord length, which has been set to avoid too blunt leading edges. Finally, the new blade has a lower stagger angle than that of the NACA blade.

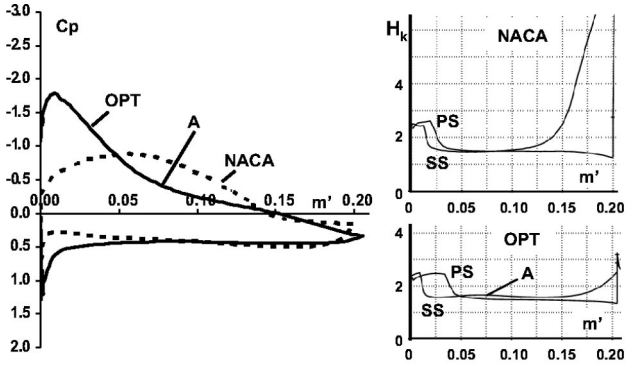

Fig. 8 Pressure distribution and form factor *Hk* of stator casing section at design point

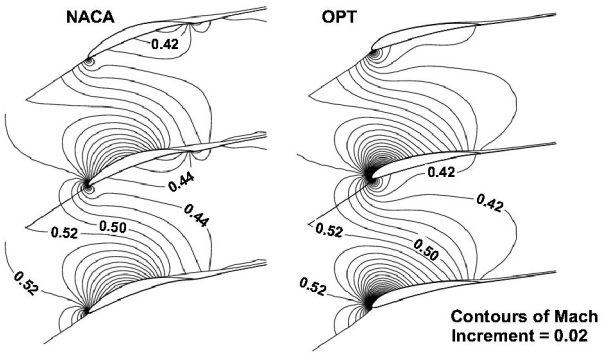

Fig. 9 Mach number distribution of stator casing section at design point

In this case all of the geometric ''killer'' criteria are fulfilled, i.e. the number of turning points (pressure side: 1; suction side: 0; **Fig. 7** right) and the cross section area and the moment of inertia (both approx. 3% above their lower limit).

Flow Features in Design Point. The positive effect of high camber and thickness close to the leading edge is demonstrated in **Fig. 8**. The flow at the suction side of the NACA profile is continuously accelerated up to a maximum at about 30% chord length (i.e. $m' = 0.05-0.06$ in **Fig. 8**) followed by a deceleration whose gradient becomes increasingly steeper towards the trailing edge. When the adverse pressure gradient is too strong for the flow to overcome, separation occurs (**Fig. 9**). Consequently, the deviation of the exit flow angle lies outside the desired tolerance and the overall pressure rise is lower.

For the optimized profile the flow on the suction side is highly accelerated and reaches its peak value shortly after the leading edge at about 5% chord length. The deceleration which follows starts with a strong gradient as in this region the boundary layer is still thin and uncritical. When the conditions start to become critical, the gradient is weakened in order to stabilize the boundary layer. This form of pressure distribution, often called ''ski-slope'' is typical for PVD and CD profiles.

The effect of stabilization can also be seen on the boundary layer form factor distribution Hk (**Fig. 8** right). After the transition, which occurs at the suction side right after the leading edge, the form factor starts to rise slowly. With the reduction of the deceleration gradient, the *Hk*-curve is flattened again and separation avoided, even though the stagger angle of the optimized profile is less than that of the NACA blade. The resulting exit flow angle is within a 0.2-deg tolerance of the desired value.

While the flow at the pressure side of the NACA blade is decelerated, the optimized profile shows an almost constant pressure distribution with a slight acceleration in the front part of the blade, which delays the transition at the pressure side and reduces the losses.

Flow Features at Off-Design. With increasing flow angle, the velocity on the suction side close to the leading edge rises as well and, in the case of the optimized profile, becomes transonic (**Fig. 10**). The higher velocity of the new profile is due to the lower stagger angle and the thickened leading edge, but, as a thicker leading edge results in less sensitivity to incidence, the velocity peak is not as distinct as for the NACA profile. The effects of the optimized pressure distribution, which have already been described for the design point (ski slope), are even more emphasized, the pressure gradient at the rear part of the blade is very small. Still, separation cannot be completely averted, but compared to the NACA blade the separation is much smaller and results in lower losses.

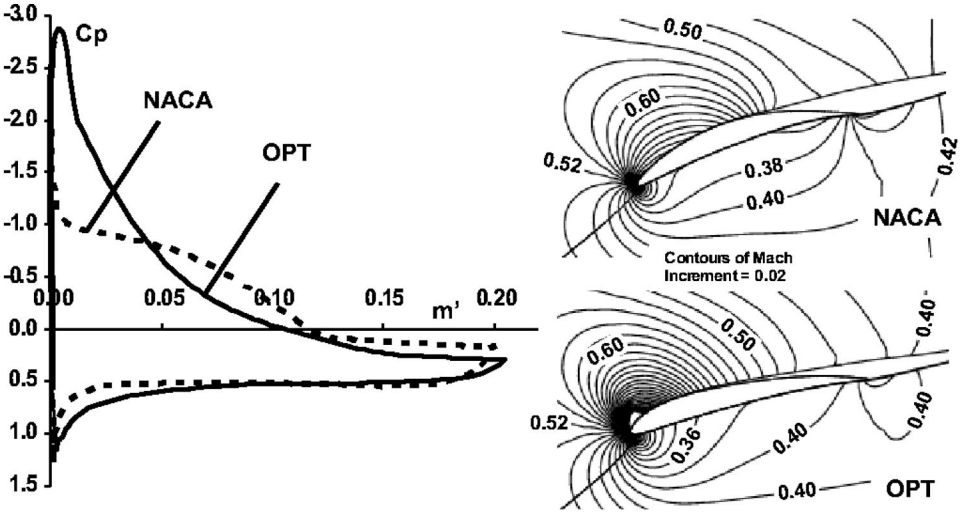

Fig. 10 Pressure and Mach number distribution of stator casing section at high inlet flow angle

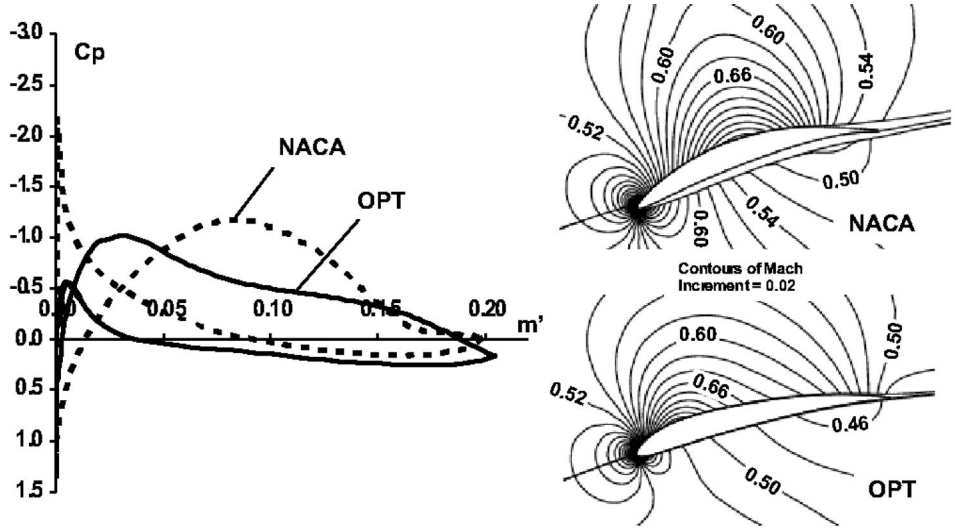

Fig. 11 Pressure and Mach number distribution of stator casing section at small inlet flow angle

The lower stagger angle of the new profile, which has been a disadvantage at high inlet flow angles, becomes advantageous for small inlet flow angles (**Fig. 11**). Due to the higher stagger angle and the thin leading edge the flow at the pressure side of the NACA blade separates immediately after the leading edge and sets therefore the lower limit of the operating range. At this point, the new blade is still working perfectly. Thanks to the smaller stagger angle and the thicker leading edge, the predicted operating range is increased by more than 50%.

Loss Coefficients. Similar results were obtained for the remaining stator and rotor sections. The loss coefficients of all sections, each compared to the corresponding NACA65 profile, are given in **Fig. 12**. For all sections the losses have been reduced significantly and the operating range increased. For the rotor hub section, it is clear that the original choice of the NACA65 profile was not at all good. The loss curve of the optimized profile is now in the desired range, while a shift to higher inlet flow angles can be found at the casing section of the rotor.

Blade Stacking

To build up the three-dimensional geometry, the centers of gravity are typically used as the stacking line for NACA65 profiles. This is possible, since all sections are members of the same profile family and their shape, and therefore the location of the center of gravity, is similar. The optimized profiles tend to have a different location of the center of gravity relative to the chord length for different sections over the span and so they are stacked over the mean value for all sections instead.

Originally, optimizations were performed for seven sections across the span of each blade. This required a lot of computing time, and the resulting shape of the blade turned out to be slightly irregular across the span. The question arose, how many sections for a proper definition of the blade were needed. To answer the question, both the rotor and the stator blades have been built up by using only the hub, midspan, and casing sections. At the span values corresponding to the four nonused sections the resulting profiles have been generated by interpolation and their loss coef-

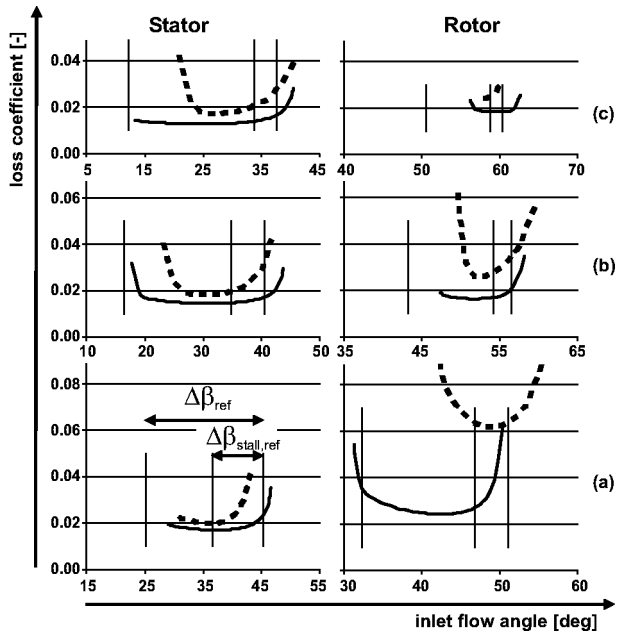

Fig. 12 Loss coefficient for (*a*) hub, (*b*) midspan, and (*c*) casing section of stator and rotor for existing (dotted) and optimized profile

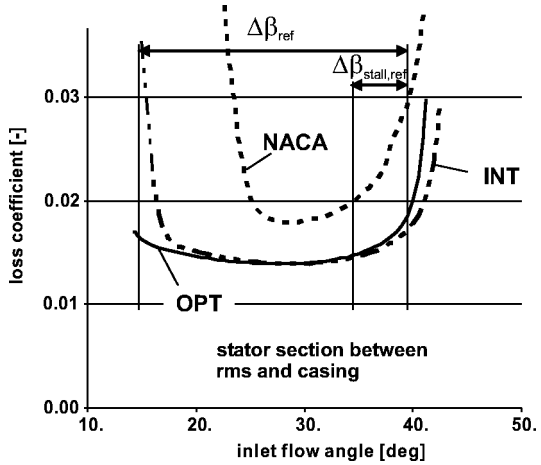

Fig. 13 Influence of number of sections used for the blade (OPT: optimized profile; INT: profile generated by interpolation)

ficients compared to those of the optimized profiles. As can be seen by the example of the stator (**Fig. 13**), the difference is only small which means that three sections per blade are sufficient for the definition of the blade.

Comparison With Three-Dimensional Navier-Stokes Simulation

In order to test the performance of the newly developed profiles, calculations were carried out using the commercial CFD package Fine/Turbo from Numeca. The geometrical model takes into account all 4 $\frac{1}{2}$ stages of the axial compressor test rig at Sulzer Innotec as well as the inlet and exit part of the machine and the tip clearances.

The mathematical model employs a steady, three-dimensional viscous turbulent Navier-Stokes solver with the Baldwin-Lomax turbulence model incorporated. Furthermore, a central discretization scheme and first order extrapolation on rotor-stator interfaces are used. The mesh consists of $\sim$2 million nodes with four possible multigrid levels. This results in average $y+$ values of $\sim$3,

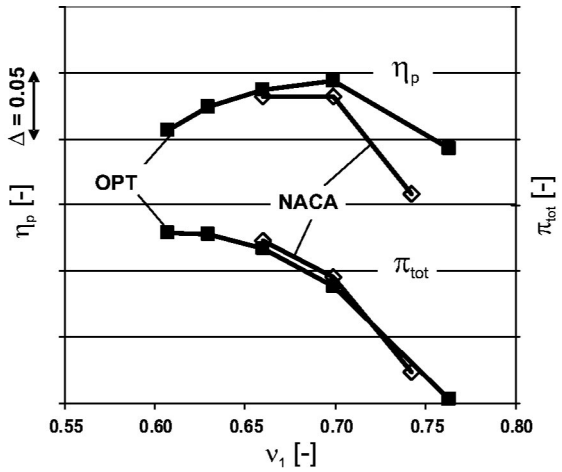

Fig. 14 Three-dimensional Navier Stokes simulations. Overall polytropic efficiency η_p and total pressure rise π_{tot} for the existing (filled squares) and the new design (diamonds).

which is required for the Baldwin-Lomax model. The calculations were performed for a machine Mach number of Mu$=$0.5 with total pressure and temperature inlet and a massflow outlet boundary condition, respectively. The calculations were considered to be converged if the difference between inlet and outlet massflow is less than 1‰, which took an average calculation time per operating point of 27 hours on an SGI octane.

The guide vane stagger angle of the existing NACA stage was chosen to be 60 deg, since this value was found by the measurements to give the highest efficiencies. For the new stage, the optimal guide vane stagger angle is not known in advance. Therefore, as an initial guess it was assumed that the difference between its design and optimum stagger angle is the same as for the NACA stage, which leads to a value of 65 deg. This assumption has to be checked by the measurements.

The overall polytropic efficiency and the total pressure rise (calculated for the 4 $\frac{1}{2}$ stages) of the existing and the new stage are presented in **Fig. 14**. The peak efficiency of the new stage is higher with a flattened characteristic and as a result an increased operating range.

Comparison With Measurements

Experimental validation of the optimised blading has been carried out in the large high-speed 4 1/2 stage axial compressor ''Palue'' in Sulzer Innotec, which has a hub diameter of 400 mm. This compressor was also used for the measurements of the original NACA 65 blading and for these new tests the annulus geometry, and all instrumentation remained unchanged, the compressor was simply fitted with a new set of blades. The instrumentation included measurement of the volume flow in a calibrated nozzle, inlet and outlet conditions (static pressures and total temperatures) upstream and downstream of the blading, and static pressures between each blade row.

Tests in this compressor follow a standard, and well-established procedure whose objective is to derive measured stage characteristics for repeating stage conditions at different stator vane stagger angle settings. In these measurements the inlet guide vane and stator vane setting angles of all blade rows are adjusted to provide a geometry that repeats through the compressor. The annulus is designed following Goede and Casey [1], and under these conditions there is one speed of the compressor which leads to repeating stage conditions through the machine at the best operating point. The establishment of repeating stage conditions can be confirmed from the static pressure measurements on the casing. At the given speed, the repeating stage conditions are then more or less retained as stall is approached, but deviate from this as choke is approached with the last stages operating at a lower relative pres-

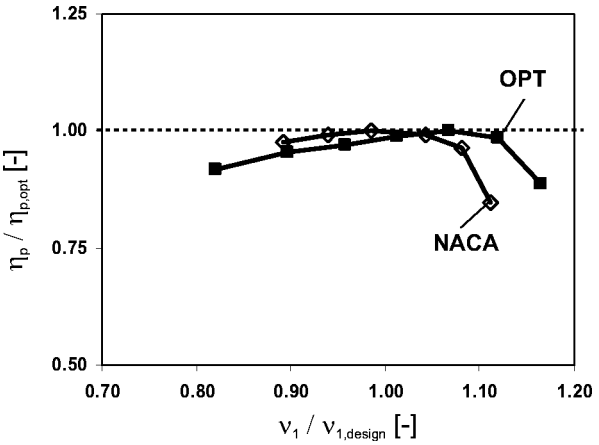

Fig. 15 Measured polytropic efficiency $\eta_p/\eta_{p,\mathrm{opt}}$ of the existing (diamonds) and the new stage (filled squares)

sure rise. Note that at higher stagger angles a lower speed is needed to attain repeating stage conditions as the stage produces a higher work input.

The measurements on this stage were completed in December 2002, during the submission process for this paper. The results, which are summarized in **Figs. 15** and **16**, are highly satisfactory with regard to the operating range of the stage, but unfortunately the optimized blading did not achieve a better efficiency than the NACA 65 blading. In the short time available since the completion of the tests it has not been possible to find an explanation for the poor efficiency of the optimised stage. Work is continuing on this.

Figure 15 shows a nondimensionalized plot of the efficiency characteristic at the design stagger angle of the optimised and the NACA 65 blading. It can be seen that the operating range of the optimised stage is significantly wider (with more than 30% more variability in flow) than that of the NACA 65 blading. **Figure 16** demonstrates that the optimized stage achieves a similar wider operating range than the NACA 65 blading at all stagger angles and speeds that have been tested. In this figure the operating range is denoted by the flow range defined as the difference between the flow coefficient at the point where the stage has 90% of its peak efficiency ($\nu_{1,90}$) and the flow coefficient at stall ($\nu_{1,\mathrm{stab}}$) divided by the design flow coefficient ($\nu_{1,\mathrm{design}}$).

$$\Delta\nu' = \frac{\nu_{1,90} - \nu_{1,\mathrm{stab}}}{\nu_{1,\mathrm{design}}} \tag{2}$$

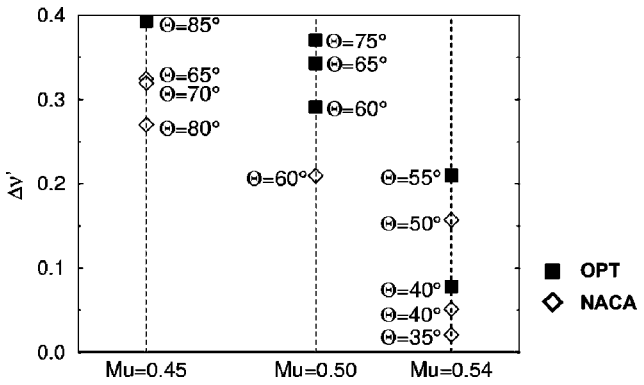

Fig. 16 Relative increase of operating range for original (NACA) and optimized (OPT) design at blade Mach number Mu=0.45, 0.50, and 0.54 and different stagger angles Θ

Conclusions

A design system for the blade sections of industrial axial compressors has been developed. The method combines a parametric geometry definition method, a powerful blade-to-blade flow solver (MISES) and an optimization technique (breeder genetic algorithm) with an appropriate fitness function. Particular effort has been devoted to the design of the fitness function for this application:

- All terms in the fitness function are nondimensional with respect to reference values.
- Essential aspects of the design (such as the required flow turning, or mechanical constraints) should not be part of the fitness function, but need to be treated as so-called ''killer'' criteria in the genetic algorithm.
- It has been found worthwhile to examine the effect of the weighting factors of the fitness function to identify how these affect the performance of the sections.
- The fitness function only includes terms related to the required performance at design and off-design operating points. Nevertheless the optimized sections have the typical velocity and boundary layer distributions associated with CD and PVD profiles.

The system has been tested on the design of a repeating stage for the middle stages of an industrial axial compressor. The resulting profiles show an increased operating range compared to an earlier design using NACA65 profiles. Three-dimensional CFD simulations and experimental measurements demonstrate the effectiveness of the new profiles with respect to the operating range.

Acknowledgments

The authors wish to thank Dr. Ernesto Casartelli for the geometry program, Rudi ter Harkel and Paul Stadler for FINE calculations, Christian Güdel for measurements, Dr. Bernhard Eisenberg for his advices.

Nomenclature

AVDR = axial velocity density ratio $=\rho_2 C_{x2}/\rho_1 C_{x1}$
CL = camber line
Cp = static pressure rise coefficient $=(p-p_1)/q$
C_x = axial velocity [m/s]
Hk = form factor $=\delta^*/\theta$
INT = interpolated profile
OPT = optimized profile
PS = pressure side
SS = suction side
U_h = blade speed at hub (m/s)
a_i = weighting factor of fitness function
e_i = weighting exponent of fitness function
k = curvature
m' = meridional coordinate $=\int[\sqrt{(dr^2+dz^2)}/r]$
p = pressure (N/m^2)
p1–p10 = parameter of camber line
p1d–p10d = parameter of thickness distribution
q = dynamic pressure at inlet (N/m^2)
r = radius (m)
rTE = trailing edge radius (m)
t = temperature (K)
x = coordinate in chordwise direction (m)
y = coordinate perpendicular to chordwise direction (m)
z = coordinate in axial direction (m)
β = flow angle with respect to axial direction (deg)
γ = ratio of specific heat capacities
$\Delta\beta$ = operating range (deg)

$\Delta\beta_{stall}$ = safety against stall (deg)
$\Delta\nu'$ = dimensionless operating range$=(\nu_{1,90}-\nu_{1,stab})/\nu_{1,design}$
δ^* = boundary layer displacement thickness (m)
η_p = polytropic efficiency (total-total)$=\gamma-1/\gamma\ \ln(p_{02}/p_{01})/\ln(t_{02}/t_{01})$
Θ = stagger angle with respect to circumferential direction (deg)
θ = boundary layer momentum thickness (m)
ν = flow coefficient$=C_x/U_h$
ρ = density (kg/m^3)
π_{tot} = stage pressure ratio$=p_{02}/p_{01}$
σ = standard deviation
ω = loss coefficient$=(p_{02,is}-p_{02})/(p_{01}-p_1)$

Subscripts

0 = stagnation value
1 = inlet plane
2 = outlet plane
80 = inner 80% of $\Delta\beta$
90 = 90% of peak efficiency
D = design point
is = isentropic
ref = reference value
stab = at stall

Superscripts

$'$ = 1st deviation
$''$ = 2nd deviation

References

[1] Goede, E., and Casey, M. V., 1988, ''Stage Matching in Multistage Industrial Axial Compressors With Variable Stagger Stator Vanes,'' VDI-Ber., **706**, pp. 229–243.
[2] Casey, M. V., 1987, ''A Mean Line Prediction Method for Estimating the Performance Characteristic of an Axial Compressor Stage,'' *Turbomachinery—Efficiency Prediction and Improvement*, Robinson College, Cambridge, UK, ImechE, London, Paper C264/87.
[3] Casey, M. V., and Hugentobler, O., 1988, ''The Prediction of the Performance of an Axial Compressor Stage With Variable Stagger Stator Vanes,'' VDI-Ber., **706**, pp. 213–227.
[4] Eisenberg, B., 1994, ''Development of a New Front Stage for an Industrial Axial Flow Compressor,'' ASME J. Turbomach., **116**, pp. 596–604.
[5] Hobbs, D., and Weingold, H., 1984, ''Development of Controlled Diffusion Airfoil for Multistage Compressor Application,'' ASME J. Eng. Gas Turbines Power, **106**, pp. 271–278.
[6] Cumpsty, N. A., 1989, *Compressor Aerodynamics*, Longman, London.
[7] Köller, U., Möning, R., Küsters, B., and Schreiber, H.-A., 1999, ''Development of Advanced Compressor Airfoils for Heavy-Duty Gas Turbines, Part I: Design and Optimization,'' ASME Paper No. 99-GT-95.
[8] Küsters, B., Schreiber, H.-A., Köller, U., and Möning, R., 1999, ''Development of Advanced Compressor Airfoils for Heavy-Duty Gas Turbines, Part II: Experimental and Theoretical Analysis,'' ASME Paper No. 99-GT-96.
[9] Sallaberger, M., Fisler, M., Michaud, M., Eisele, K., and Casey, M. V., 2000, ''The Design of Francis Turbine Runners by 3-D Euler Simulations Coupled to a Breeder Genetic Algorithm,'' 20th IAHR Symposium on Hydraulic Machinery and Systems, Charlotte, NC, Aug.
[10] Casey, M. V., April 1983, ''A Computational Geometry for the Blades and Internal Flow Channels of Centrifugal Compressors,'' ASME J. Eng. Gas Turbines Power, **105**, pp. 288–295.
[11] Youngren, H., and Drela, M., 1991, ''Viscous/Inviscid Method for Preliminary Design of Transsonic Cascades,'' Paper No. AIAA-91-2364.
[12] Abu-Ghannam, B., and Shaw, R., 1980, ''Natural Transition of Boundary Layers. The Effects of Turbulence, Pressure Gradient and Flow History,'' J. Mech. Eng. Sci., **22**, pp. 213–228.
[13] Mühlenbein, H., and Schlierkamp-Voosen, D., 1993, ''Predictive Models for the Breeder Genetic Algorithm I. Continuous Parameter Optimisation,'' Evol. Comput., **1**, pp. 25–49.
[14] Mühlenbein, H., and Schlierkamp-Voosen, D., 1994, ''The Science of Breeding and Its Application to the Breeder Genetic Algorithm,'' Evol. Comput., **1**, pp. 335–360.